Journal of Hazardous Materials 201–202 (2012) 265–272

Contents lists available at SciVerse ScienceDirect

Journal of Hazardous Materials

journal homepage: www.elsevier.com/locate/jhazmat

An alternative approach to recovering valuable metals from zinc phosphating sludge

Yi-Ming Kuo*

Department of Safety Health and Environmental Engineering, Chung Hwa University of Medical Technology, Tainan City, 71703, Taiwan, ROC

ARTICLE INFO

Article history:
Received 22 August 2011
Received in revised form 27 October 2011
Accepted 24 November 2011
Available online 1 December 2011

Keywords:
Zinc phosphating sludge
Recovery
Vitrification
Amorphous
Basicity

ABSTRACT

This study used a vitrification process (with good potential for commercialization) to recover valuable metals from Zn phosphating sludge. The involved vitrification process achieves two major goals: it transformed hazardous Zn phosphating sludge into inert slag and it concentrated Fe (83.5%) and Zn (92.8%) into ingot and fine particulate-phase material, respectively. The Fe content in the ingot was 278,000 mg/kg, making the ingot a potential raw material for iron making. The fine particulate-phase material (collected from flue gas) contained abundant Zn (544,000 mg/kg) in the form of ZnO. The content (67.7%) of ZnO was high, so it can be directly sold to refineries. The recovered coarse particulate-phase material, with insufficient amount of ZnO, can be recycled as a feeding material for Zn re-concentration. Therefore, the vitrification process can not only treat hazardous materials but also effectively recover valuable metals.

1. Introduction

Phosphating is widely used in the metal pretreatment processes for the surface finishing of ferrous and nonferrous metallic components. It can yield excellent wear resistance, corrosion resistance, adhesion, and lubrication properties in an economic and rapid way [1,2]. Among these phosphating technologies, Zn phosphating coated components exhibit good corrosion resistance and can endure severe environments [3]. Therefore, this technology is often used to produce components in automotive and electronics industries.

In general, three main reactions involve in a zinc phosphating process: pickling, coating, and sludge reactions [4]. A pickling reaction (reaction (1)) occurs when zinc phosphate solution contacts the surface of a plated object; by this way, H^+ ions may dissolve some metals on the object's surface. This reaction is essential for the coating formation because it cleans the surface and improves the adhesion of the coating of the base metals.

$$Fe + 2H^+ + 2O_x \rightarrow Fe^{+2} + 2HO_x \quad (1)$$

O_x: oxidation agents (used as accelerators for the pickling reaction)

For the coating reaction, the pH rises due to the consumption of H^+ ions in the pickling reaction. Metal cations react with the phosphate in the solution and become deposited on the object's surface as crystalline zinc phosphate (reaction (2)).

$$2Zn^{+2} + Fe^{+2} + 2H_2PO_4^- \cdot 4H_2O \rightarrow Zn_2Fe(PO_4)_2 \cdot 4H_2O + 4H^+ \quad (2)$$

After the coating reaction, Fe^{+2} ions from the pickling reaction are oxidized by oxidative reagents and precipitate as sludge (reactions (3) and (4)). As a result, residual Zn^{+2} ions are incorporated into the solution from the dissolution of zinc phosphate during the coating reaction and do not form any sludge.

$$Fe^{+2} + H^+ + O_x \rightarrow HO_x + Fe^{+3} \quad (3)$$

$$Fe^{+3} + H_2PO_4^- \rightarrow FePO_4 + 2H^+ \quad (4)$$

According to reactions (2)–(4), Zn^{+2} should not be precipitated to form sludge after the final reaction. However, the disposal (often by coagulation and flocculation) of spent zinc phosphate solution often makes the Zn^{+2} ions concentrated into iron phosphate sludge [5]. Consequently, the sludge generated in the zinc phosphating process usually contains high levels of Fe and Zn, which are valuable metals. A conventional method for treating the phosphating sludge is solidification followed by landfill. This prevents the metals from being reused and may cause secondary environmental pollution. Therefore, it is attractive to recover these valuable metals from phosphating sludge.

Vitrification is usually used to stabilize hazardous materials, such as fly ash, radioactive waste, spent alkaline batteries, and spent catalysts [6–9]. Although vitrification is a high-energy-consuming and high-cost technology, it has some major advantages over other methods [10]. It can effectively immobilize toxic metals and

* Corresponding author. Tel.: +886 6 2674567x854; fax: +886 6 2675049.
E-mail addresses: yiming@mail.hwai.edu.tw, kuoyiming@gmail.com

0304-3894/$ – see front matter © 2011 Elsevier B.V. All rights reserved.
doi:10.1016/j.jhazmat.2011.11.081

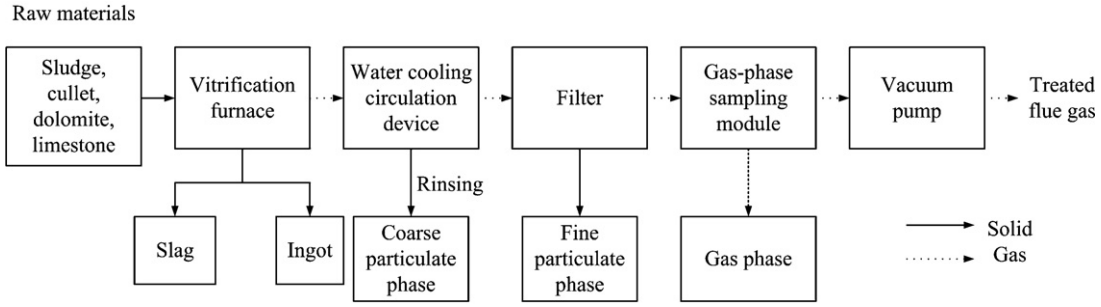

Fig. 1. Flow chart of the vitrification system.

transform hazardous waste into stabilized slag [11]. It can also decompose organic pollutants, such as polycyclic aromatic hydrocarbons (PAHs) and dioxins, to prevent secondary pollution [12]. For raw materials rich in precious metals, vitrification can recover the metals in the form of ingot [13].

A previous study reported that Cr electroplating sludge can be vitrified with cullet and incineration bottom ash [14]. The sludge was transformed into stable slag with low hazardous metal leaching ratios. However, most of the Cr was encapsulated in the slag in the form of Cr_2O_3 and could thus not be recovered. The objective of the present study is to stabilize zinc phosphating sludge and recover Fe and Zn from the sludge. Therefore, we examine if these two metals in zinc phosphating sludge could be transformed into recoverable forms via the high temperature treatment during vitrification. The metal compositions of input and output materials were analyzed and the crystalline characteristics of the products were examined. In addition, the fates of Fe and Zn during the vitrification process were investigated to determine the feasibility of using vitrification to recover such metals.

2. Experimental

2.1. Raw material preparation

Zinc phosphating sludge was sampled from a Zn coating factory in southern Taiwan. The sludge was dried at 105 °C for 1 day to remove water content. Additives, namely cullet, dolomite ($CaCO_3{\cdot}MgCO_3$), and limestone ($CaCO_3$), were pulverized and added before vitrification. The first and the latter two acted as a glass former and glass modifiers, respectively. According to the results of a previous study, additives with a mixed mass ratio of dolomite: limestone: cullet = 1:3:4 were adopted [8]. According to the composition of additives, the basicity of each specimen (mass ratio of CaO/SiO_2 before vitrification) was controlled at 0.6 in such a mixed mass ratio. The additive ratio (AR, defined as total additive mass/input material mass) was used as an operating parameter to examine the separation efficiency of Fe. The sludge and additives were mixed with ARs of 0.1, 0.2, 0.3, and 0.4 to evaluate the effect of ARs on the metal recovery; after vitrification, the correspondingly obtained slags were named S-1 to S-4 respectively. In the round of AR = 0.2, the output materials in the flue gas were specifically analyzed to investigate the distribution of metals.

The involved vitrification system was a modified version of that used in a previous study [8]. A flow chart of the system is shown in Fig. 1. The premixed powdery specimens were held in graphite crucibles and heated using a vitrification furnace. The furnace has inner space dimensions of 25 cm × 25 cm × 20 cm; it is coated with refractory materials and equipped with four Si_2Mo heating rods. The furnace is electrically heated (220 V × 30 A) and the maximum operation temperature is 1600 °C. The temperature program is: heating from 30 to 1000 °C at a heating rate of 6 °C/min, heating from 1000 to 1450 °C with a heating rate of 4 °C/min, isothermal holding at 1450 °C for 1 h, and cooling to room temperature. The energy consumption for the vitrification process was about 20 kWh. The cooled solid specimens were separated by gravity into two parts (slag and ingot) according to their physical characteristics. During vitrification, molten materials with higher density crept toward the bottom and gathered as ingot after cooling, whereas the residual fraction floated to the upper layer and formed slag after cooling. The flue gas was pumped from the top outlet through a water-cooling circulation device to reduce the temperature to under 70 °C. The particulate phase and gas phase metals in the flue gas were sampled by a filter and a gas-phase sampling module, respectively.

2.2. Gas phase sampling

The flue gas was sampled using a pump (1AM, Gast) with a flow rate of 3 L/min. The flow rates before and after sampling were measured and averaged as mean flow rates to determine the total sampled gas volume. The metal species in the flue gas were divided into particulate-phase and gas-phase metals. In the cooling down process, some coarse particulate matter adhered to the inner wall of the stainless steel tubes connecting the vitrification furnace and water-cooling circulation device, with the remaining coarse particulate matter adhering to the water circulation tubes. An acid solution of 0.1 N HNO_3 was used to rinse the tube walls. The washed solution was digested, filtrated, and then analyzed to measure the metal mass, which was taken as coarse particulate-phase metals. Glassfiber filters, following the water cooling circulation device, were used to collect the fine particulate matter. The glassfiber filters (Tissuquartz, 2500QAT-UP) (made of pure quartz) with the diameter of 51 mm, thickness of 432 μm (17 mils), and specific weight of 5.8 mg/cm^2, can capture 99.9% aerosols during sampling. Each filter was conditioned and precisely weighed before and after sampling to measure the particulate matter mass. The sample was then digested and analyzed to determine the metal mass, which was regarded as fine particulate-phase metals. After the filter, the flue gas passed through five impingers serially connected in a module (Fig. 2), for sampling the gas-phase metals. Impingers 1 and

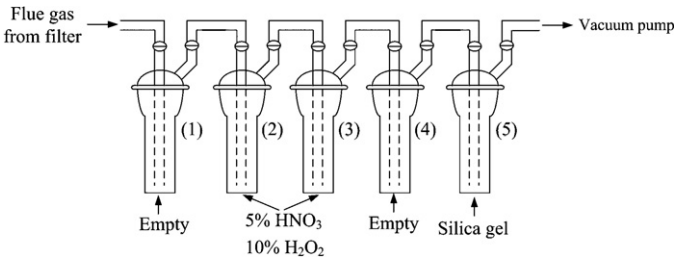

Fig. 2. The impinger module used for gas-phase metal sampling.

4 were empty, impingers 2 and 3 were filled with a solution of 5%HNO_3 + 10%H_2O_2, and impinger 5 was filled with silica gel. The experimental procedure followed the standard method for gas-phase sampling given in Taiwan EPA NIEA A302.72C [15]. The metal concentrations of the solutions were then analyzed using atomic absorption spectrometry (AAS) to calculate the gas-phase metal mass.

2.3. Digestion procedure

The solid specimens, namely zinc phosphating sludge, cullet, dolomite, limestone, slag, ingot, and particulate matter, were all digested in triplicate for subsequent instrumental analysis. The standard method given in the USEPA Method Study 37-SW-846 Method 3050b was modified to improve the digestion efficiency [16]. Specimens were pulverized to a size, which can pass a mesh-100 sieve (148 μm) to ensure consistent digestion. Each powdery specimen (0.3 g) was added to an acid mixture of 1 mL HF (hydro fluoride) + 3 mL HCl (hydro chloride) + 5 mL HNO_3 (nitric acid), held in a sealed Teflon vessel, and digested by a microwave digester (MARS Xpress, CEM). The specimens were heated from 30 °C to 180 °C at a rate of 10 °C/min, held isothermally for 1 h, and cooled down to room temperature. The digests were diluted to 50 mL with deionized water, filtrated by a mixed cellulose ester filter, and then analyzed using AAS.

2.4. Toxicity characteristics leaching procedure

The toxicity characteristics leaching procedure (TCLP) was used to assess the metal mobility of the slag. The leaching, dilution, and digestion procedures followed the standard method stated in the USEPA Method 1311 [17]. The digests were then analyzed by AAS.

2.5. Instrumental analysis

AAS (Sens AA, GBC) was used to analyze the metals in the solutions of impingers and the digests of solid specimens and TCLP samples. The concentrations of Al, Ca, Cd, Cr, Co, Cu, Fe, K, Mg, Mn, Ni, Pb, and Zn in these solutions were measured in triplicate for each sample to obtain an average value and relative standard deviation (RSD = (standard deviation/average) × 100%).

2.6. Analysis of surface and crystalline characteristics

Scanning electron microscopy–energy dispersive spectroscopy (SEM–EDS, JEOL JXA-840) was used to examine the surface characteristics of solid specimens. Powdery specimens (smaller than 74 μm) were stuck on a metallic plate and coated with a film of Au using an ion coating sputter. Electron beams accelerated with a voltage of 25 kV were used to scan the specimens' surface with a magnification factor of 10,000.

An X-ray powder diffractometer (XRD, Geigerflex 3063) with Ni-filtered Cu-Kα radiation was used to determine the crystalline phases (CPs) of solid specimens. The solid specimens were pulverized to a particle size smaller than 74 μm, mixed with high-purity silica powder with a Si/specimen mass ratio of 0.1 to serve as an internal standard, and measured in the 2θ range of 10–60° at an angular speed 4°/min. The internal standard served as an indicator of the amount of CP in the semi-quantitative XRD analysis [18]. The amount of CP is approximately proportional to the summation of the area under crystalline peaks, and thus, each crystalline phase was semi-quantitatively measured by comparing the total area under crystalline peaks with that under Si peaks. The semi-quantitative XRD analysis, described in detail in a previous study [19], was used to measure the crystalline characteristics of slag [11].

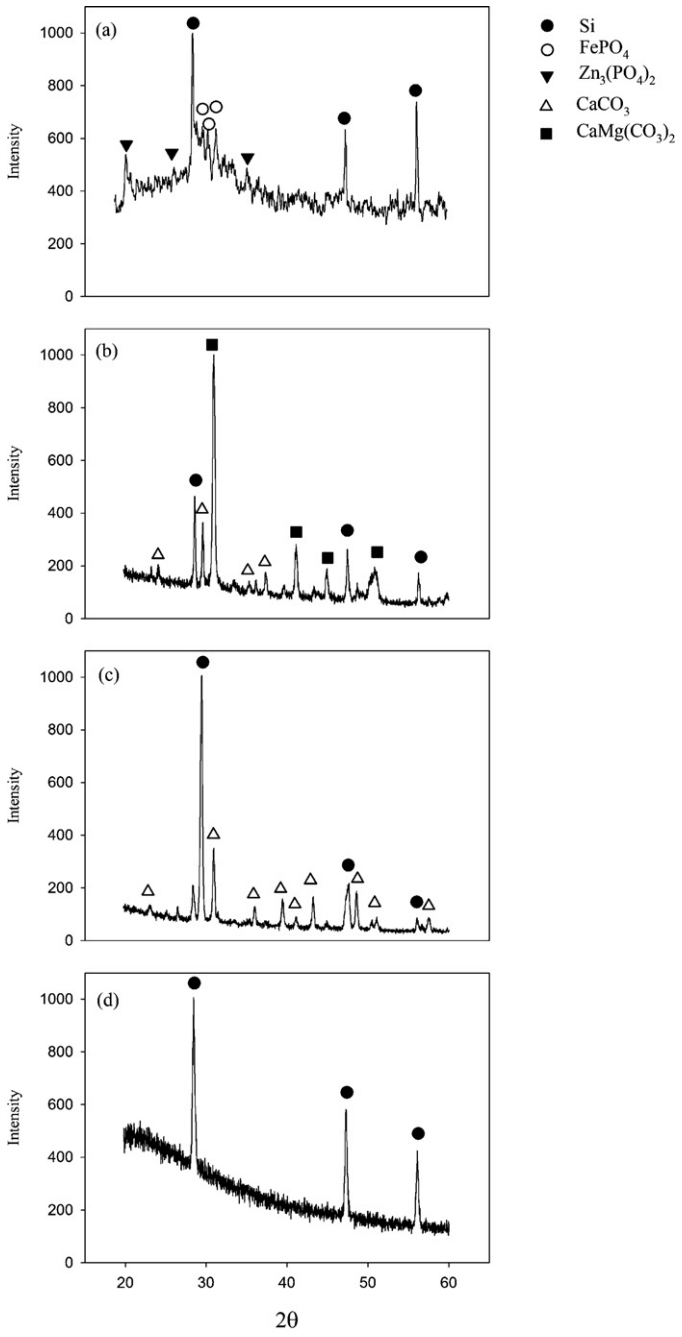

Fig. 3. XRD patterns of input materials: (a) Zn phosphating sludge, (b) dolomite, (c) limestone, and (d) cullet.

The amorphous volume fraction (AVF) of the specimens was then calculated using the following equation:

$$\mathrm{AVF} = 1 - \sum_{i=1}^{n} \mathrm{CP}_i \tag{5}$$

CP_i: the volume fraction of the ith crystalline phase.

3. Results and discussion

3.1. Characteristics of input materials

The compositions and the XRD analysis diagrams of input materials are shown in Table 1 and Fig. 3, respectively. The Zn

Table 1
Compositions of input materials.

Item	Sludge		Dolomite		Limestone		Cullet	
	Average (mg/kg)	RSD (%)	Average (mg/kg)	RSD (%)	Average (mg/kg)	RSD (%)	Average (mg/kg)	RSD (%)
Al	0.667	50.0	134	40.79	61.5	5.62	652	14.2
Ca	378	70.0	217,000	9.99	385,000	2.01	15,000	58.1
Cd	16.6	2.32	8.43	34.9	5.30	6.54	20.3	111
Cr	196	4.97	7.27	19.0	11.2	13.9	4.41	12.0
Co	56.2	3.62	N.D.	–	N.D.	–	47.5	16.7
Cu	5.67	29.4	0.650	173	15.3	97.7	N.D.	–
Fe	81,500	9.49	1260	1.47	1250	0.551	582	1.80
K	200	11.4	N.D.	–	77.8	13.8	1710	25.6
Mg	19.6	22.5	129,000	31.8	444	15.2	53.5	62.3
Mn	40.0	20.4	14.1	9.36	177	30.2	16.4	3.77
Ni	510	8.08	16.6	20.2	22.2	5.15	N.D.	–
Pb	53.2	29.0	96.9	8.16	96.7	8.70	107	6.43
Si	8110	23.2	40	10.1	46	15.2	396,000	20.3
Zn	73,600	2.32	2110	21.8	29.9	17.2	80.3	76.3
AVF (%)	59.4	–	43.2	–	39.9	–	93.4	–
PCP	$Zn_3(PO_4)_2$/Fe PO_4	–	$CaCO_3$	–	$CaCO_3 \cdot MgCO_3$	–	None	–
PCP amount	3.92/4.17	–	56.8	–	52.5	–	–	–

N.D.: not detectable; –: not available.

phosphating sludge is mainly composed of Fe (81,500 mg/kg) and Zn (73,600 mg/kg), which mainly existed in the forms of phosphate. Dolomite has two predominant metal species, Ca (217,000 mg/kg) and Mg (129,000 mg/kg); its predominant CP is $CaCO_3 \cdot MgCO_3$. Calcium (385,000 mg/kg) is the major element of limestone while Si (396,000 mg/kg) is the major element of cullet. The metal content of dolomite and limestone coincided with their CPs in XRD patterns. No predominant CP was found in the XRD analysis for cullet. The AVF for cullet was high (93.4%), indicating that it had an amorphous structure.

Table 2 shows the metal mass contributions of input materials. Anthropogenic metals, Cd (65.3%), Co (78.0%), Cu (59.4%), Fe (99.3%), Ni (98.7%), Pb (43.9%), and Zn (99.7%), predominately came from the Zn phosphating sludge. Crust metals were mainly contributed by additives. Limestone and dolomite donated 80.4% of Ca and 98.6% of Mg, respectively. Cullet contributed most of Al (72.4%), K (72.2%), and Si (61.9%). The metal mass distribution elucidated that additives provide crust metals, which formed structures (during vitrification) to encapsulate and immobilize anthropogenic metals from mainly the Zn phosphating sludge.

3.2. Characteristics of output materials

The compositions and the XRD analysis diagram of output materials are given in Table 3 and Fig. 4, respectively. The slag was mainly composed of Ca (247,000 mg/kg) and Si (201,000 mg/kg). The XRD patterns of other slags were all highly amorphous and no significant crystalline phases were identified. The crystalline profiles of slags were all similar, and thus, S-2 (AVF = 90.8%) was used to represent the other slags. For ingot, the major component was Fe (278,000 mg/kg). The concentration of Ca and Si were 2060 and 2070 mg/kg, respectively, which are much lower than those in the slag. The variation of element levels shows that Fe moved toward the bottom of specimens and was retained by ingot whereas the residual fraction, rich in Ca and Si, stayed at the upper layer and was retained by slag. The separation of metal species can be explained by the creeping of molten materials, which results from the differences of metal densities. According to the XRD patterns, Fe existed primarily as Fe_2P, Fe_2O_3, and Fe_3O_4, which can be used as raw materials for iron making [20].

Table 2
Metal mass of input materials (AR = 0.2).

Element	Sludge (%)	Dolomite (%)	Limestone (%)	Cullet (%)
Al	0.2	22.2	5.1	72.4
Ca	0.3	15.1	80.4	4.2
Cd	65.3	2.8	5.2	26.7
Cr	97.6	0.3	1.4	0.7
Co	78.0	0.0	0.0	22.0
Cu	59.4	0.6	40.1	0.0
Fe	99.3	0.1	0.4	0.2
K	25.3	0.0	2.5	72.2
Mg	0.2	98.6	1.0	0.2
Mn	44.0	1.3	48.7	6.0
Ni	98.7	0.3	1.1	0.0
Pb	43.9	6.7	20.0	29.5
Si	38.0	0.0	0.1	61.9
Zn	99.7	0.2	0.0	0.0

The metal profiles of the coarse and fine particulate-phases were similar. Both ashes were mainly composed of Zn, Pb, K, and Ca and had some other common metals, such as Al, Cd, and Fe, in trace amounts. The Zn concentrations were 136,000 and 544,000 mg/kg in the coarse and fine particulate-phases, respectively. During vitrification, dolomite and limestone were decomposed to oxides and CO_2 (reactions (6) and (7)). CO_2 reacted with C, which came from the graphite crucible and was then transformed into CO (reaction (8)).

$$CaCO_3 \xrightarrow{\Delta} CaO + CO_2 \quad (6)$$

$$MgCO_3 \xrightarrow{\Delta} MgO + CO_2 \quad (7)$$

$$CO_2 + C \rightarrow 2CO \quad (8)$$

CO could reduce metal ions (Fe^{+3} and Zn^{+2}) to elementary forms. However, metals stayed in slag or ingot might be oxidized again when the specimens was cooled down to room temperature. During the cooling process, Fe ions would combine with oxygen or phosphorous, which were probably reduced from phosphate, and, thus, existed as oxide or phosphide. For Zn, it was oxidized again while vaporizing into the flue gas and existed as oxide (ZnO).

According to the XRD analysis, both ashes existed mainly as ZnO, which verified the above inference. The collected coarse particulate-phase material was highly amorphous (its AVF was 94.6%); the volume fraction of ZnO was only 3.07%. This shows that some amorphous impurities resulted in the insufficiently high content of coarse particulate-phase Zn for its direct recovery. Nevertheless, Zn can be reconcentrated by recycling the coarse particulate-phase material back into the vitrification furnace. For fine particulate-phase material, the content (67.7%, converted from Zn) of ZnO was high enough for the ZnO to be directly sold to metal recovery factories for further refinement [21].

Table 3
Compositions of output materials (AR = 0.2).

Item	Solid				Flue gas					
	Slag		Ingot		Coarse particulate-phase		Fine particulate-phase		Gas phase	
	Average (mg/kg)	RSD (%)	Average (mg/kg)	RSD (%)	Average (mg/kg)	RSD (%)	Average (mg/kg)	RSD (%)	Average (mg/kg)	RSD (%)
Al	507	49.3	22.8	36.2	688	102	30.6	7.34	0.2	45.4
Ca	247,000	40.0	2060	17.0	20,800	82.0	6800	5.52	66.8	98.7
Cd	14.7	38.0	1.69	91.0	1890	68.5	625	9.34	9.6	55.6
Cr	151	18.6	1190	85.1	N.D.	–	N.D.	–	16.5	30.5
Co	27.3	6.90	240	39.4	175	77.9	48.9	10.5	2.8	47.9
Cu	6.93	76.7	87.1	27.6	250	78.0	50.3	28.4	2.6	92.1
Fe	15,100	22.6	278,000	18.1	3660	66.4	937	55.5	5.3	123
K	359	23.1	102	31.9	24,600	70.0	4520	12.4	258	78.3
Mg	14,100	5.86	85.1	34.2	81.3	96.1	12.6	89.2	7.0	124
Mn	99.2	24.0	574	19.5	20.5	76.2	15.0	39.7	N.D.	–
Ni	633	27.8	795	21.3	288	89.7	37.8	51.0	4.4	82.4
Pb	43.9	49.9	46.4	19.2	16,500	17.0	14,900	27.5	10.3	107
Si	201,000	15.4	2070	32.2	250	25.4	240	18.6	7.4	38.1
Zn	393	76.9	18.4	35.1	136,000	45.7	544,000	7.84	3760	27.3
AVF (%)	90.8	–	49.5	–	94.6	–	56.5	–	–	–
PCP	None	–	Fe_2P/Fe_2O_3	–	ZnO	–	ZnO	–	–	–
PCP amount	–	–	20.0/3.70	–	3.07	–	12.1	–	–	–

N.D.: not detectable; –: not available.

3.3. Mass distribution of output materials

Table 4 presents the metal distribution of output materials. After vitrification, anthropogenic metals with high boiling points and densities, including Cr, Co, Fe, and Mn, moved into the ingot, whereas crust metals with high boiling points and low densities, such as Al, Ca, Mg, and Si, tended to stay in the slag. Other anthropogenic metals with low boiling points, including Cd, Pb, and Zn, went into the flue gas, so they mostly stayed in the particulate-phase. According to the metal distribution, it is inferred that the boiling points and densities of metals governed the movement of molten materials during the vitrification process. With a gradual increase in temperature, metals with low boiling points vaporized as the particulate phase into flue gas and the residual specimen started to melt and creep. For the molten materials, metals with higher densities sank down to the bottom layer and formed ingot while other metals stayed at the upper layer to produce slag. The separation of slag and ingot was due to the gravity effect. The distribution pattern was similar to those reported in a previous study [22].

According to the sampling characteristics of particulate-phase materials, coarse and fine particulate-phases should be trapped by cyclone and baghouse filters in a full-scale operation. 2.54% and 92.8% of Zn distributed in the coarse and fine particulate-phase materials, respectively. This means that most of Zn may be collected using baghouse filters. In addition, the recycling of coarse particulate-phases back into the vitrification process would not have a significant influence on the recovery of Zn. The results show that this vitrification process can be applied to recover low boiling point metals (Cd, Hg, Pb, or Se) from metal-enriched wastes.

3.4. Separation behavior

Fig. 5 shows the DTG (differential thermal gravity) curve and the Zn evaporation behavior versus temperature. According to the slope of the DTA curve, the evaporation behavior of Zn phosphating sludge can be divided into four stages: (I) organic decomposition stage, (II) steady state stage, (III) initial high temperature vaporization stage, and (IV) final high-temperature vaporization stage.

3.4.1. Stage I (organic decomposition stage)

The sludge mass decreased by 20% in this stage, but the mass of Zn did not change notably. In a phosphating process, many organic chemicals are added to the bath solution to remove grease or to clean the component surface [23]. Then the waste solution, containing metal ions and organic compounds, is coagulated by adding a polymer, followed by the adjustment of pH using NaOH, before discharging as effluent [24]. Accordingly, it is reasonable that organic compounds were present in the Zn phosphating sludge in this study. These organics decomposed from 0 to 400 °C, accounting for about 20% sludge mass loss (Fig. 5, top).

Table 4
Metal mass distribution of output materials (AR = 0.2).

Element	Slag (%)	Ingot (%)	Coarse particulate-phase (%)	Fine particulate-phase (%)	Gas phase (%)
Al	96.0	1.20	2.00	0.74	0.03
Ca	99.3	0.23	0.12	0.35	0.02
Cd	19.6	0.63	22.6	46.8	10.36
Cr	30.5	66.8	0.00	0.00	2.70
Co	26.0	63.6	2.26	5.93	2.18
Cu	24.2	42.8	13.2	12.5	7.32
Fe	16.3	83.5	0.05	0.13	0.00
K	34.6	2.74	15.9	26.5	20.3
Mg	99.8	0.17	0.01	0.01	0.04
Mn	38.0	61.1	0.12	0.73	0.00
Ni	73.1	25.5	0.43	0.55	0.41
Pb	24.3	7.15	29.5	34.4	4.67
Si	98.7	0.28	0.1	0.9	0.00
Zn	0.5	0.01	2.54	92.8	4.10

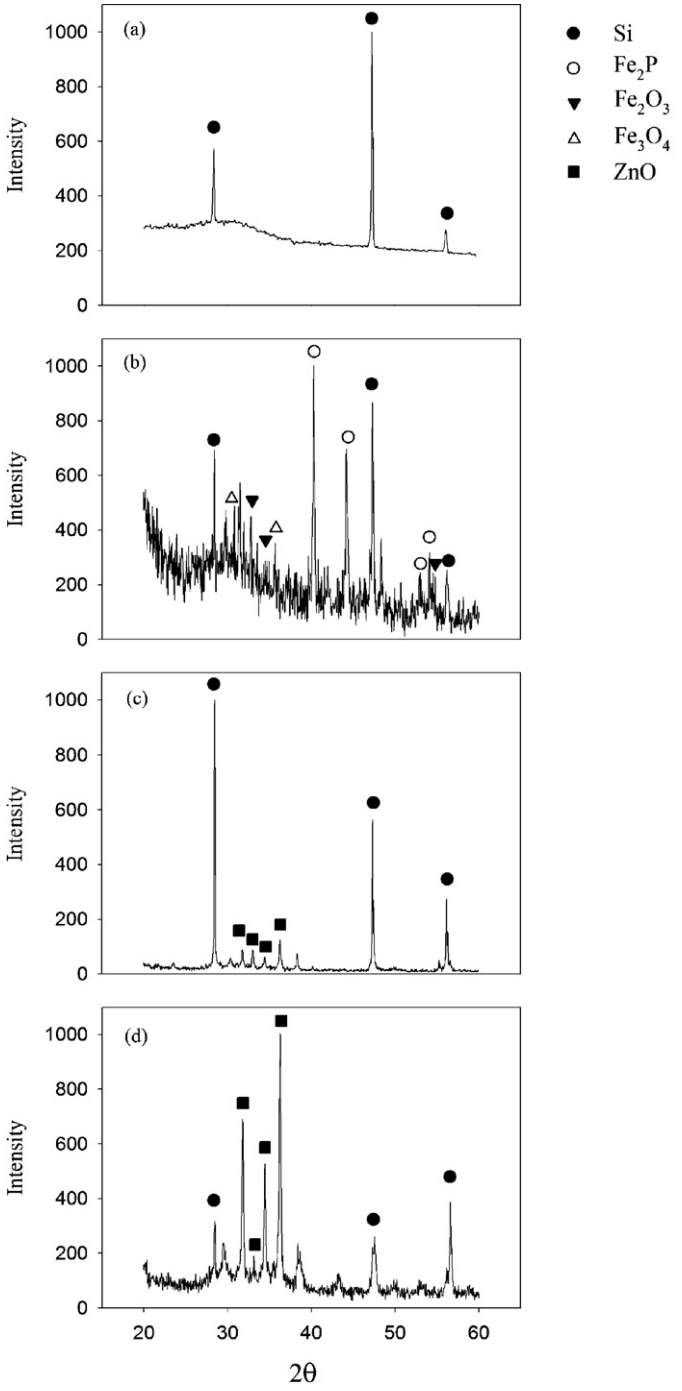

Fig. 4. XRD patterns of output materials (AR = 0.2): (a) slag, (b) ingot, (c) coarse particulate-phase material, and (d) fine particulate-phase material.

3.4.2. Stage II (stable stage)

In the temperature range of 540–1195 °C, no significant variation of sludge mass was observed, so the sludge mass was relatively stable in comparison to the other stages.

3.4.3. Stage III (initial high-temperature vaporization stage)

Above 1195 °C, the sludge and Zn both started to vaporize at constant rates, but the vaporization rate was much lower for the former than for the latter. Thus, in this stage, the mass reduction of the sludge resulted mainly from the vaporization of Zn. Other inorganic compounds did not vaporize in this temperature range.

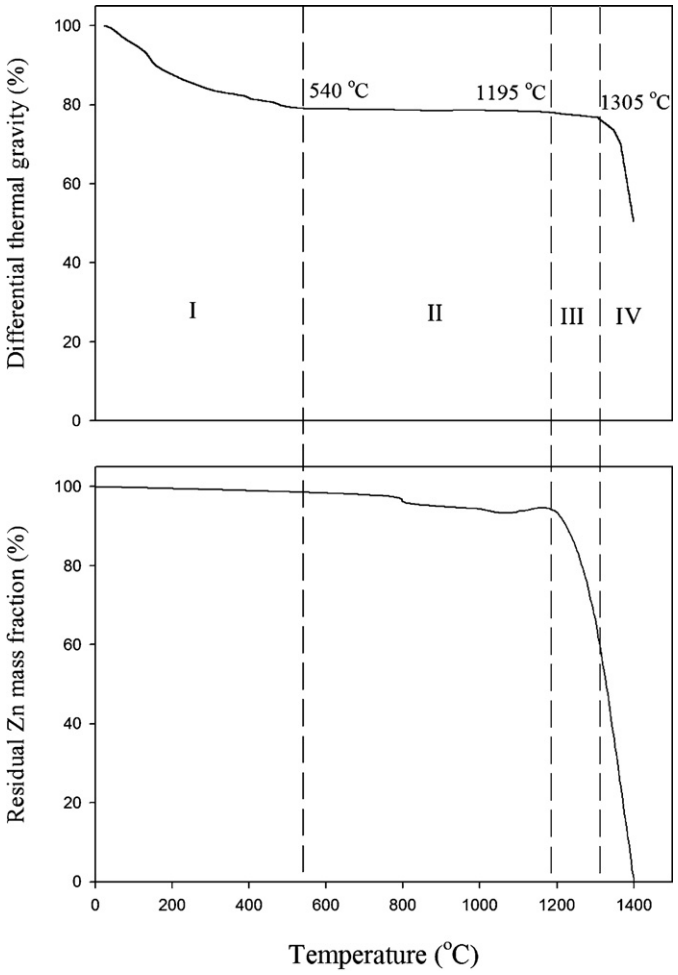

Fig. 5. Mass variation of Zn phosphating sludge and Zn during vitrificaiton.

3.4.4. Stage IV (final high-temperature vaporization stage)

When the temperature increased to ≥1300 °C, the sludge mass decreased drastically and the mass reduction was 50% when the temperature reached 1400 °C (Fig. 5, bottom). At this condition, only trace amount of Zn in the sludge was detected, so it almost completely separated from the sludge and was present as particulate-phase material in the flue gas.

For the recovery of valuable metals with high densities and boiling points, it is necessary to concentrate them into ingot. Therefore, an index used to describe the separation efficiency of Fe (SE_{Fe}) was defined as below:

$$SE_{Fe} = \frac{m_{ingot}}{m_{ingot} + m_{slag} + m_{flue\ gas}} \times 100\% \quad (9)$$

m_i: Fe mass in the ith product.

Fig. 6 displays the SE_{Fe} and the slag AVF versus AR. The SE_{Fe} was initially 0.77 and then increased with the increase of AR. At 0.87 (AR ≈ 0.3), SE_{Fe} started to decrease with an increasing amount of additive. The variation of SE_{Fe}, similar to that of slag AVF, initially increased, then reached its highest value at AR ≈ 0.26, and lastly decreased. When comparing the two diagrams of SE_{Fe} and the slag AVF versus AR, the trends of the two regression lines in Fig. 6 are very similar. This phenomenon reveals that Fe was efficiently separated from the sludge and moved into ingot at appropriate AR values, but excess additive had an adverse effect on the separation of Fe from the sludge. It was also observed that higher AVF in the slag led to more Fe moving into the ingot. In the vitrified structure with a higher AVF, inorganic compounds were commonly

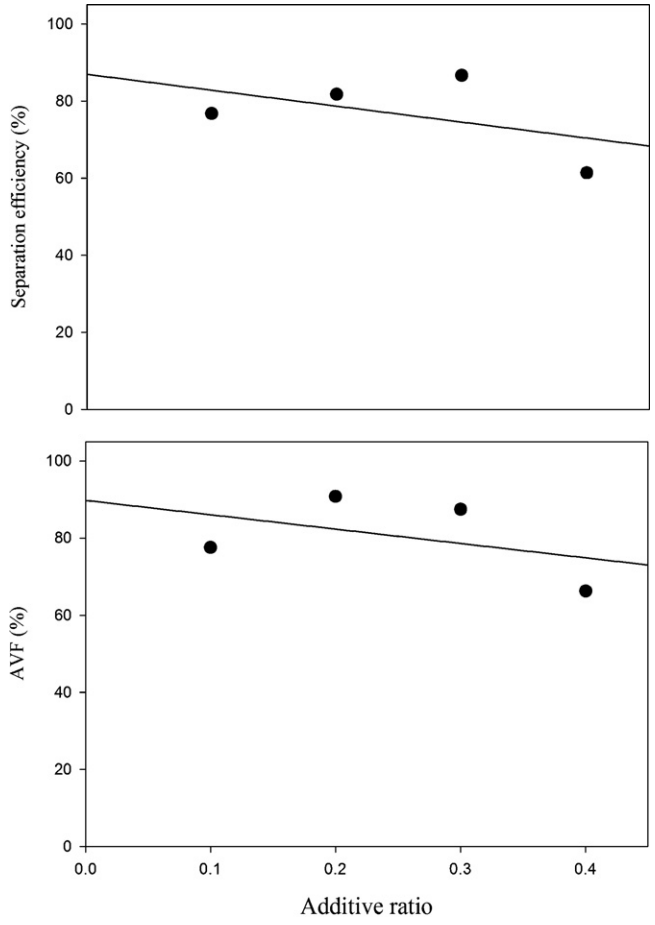

Fig. 6. Separation efficiency of Fe and AVF of slags.

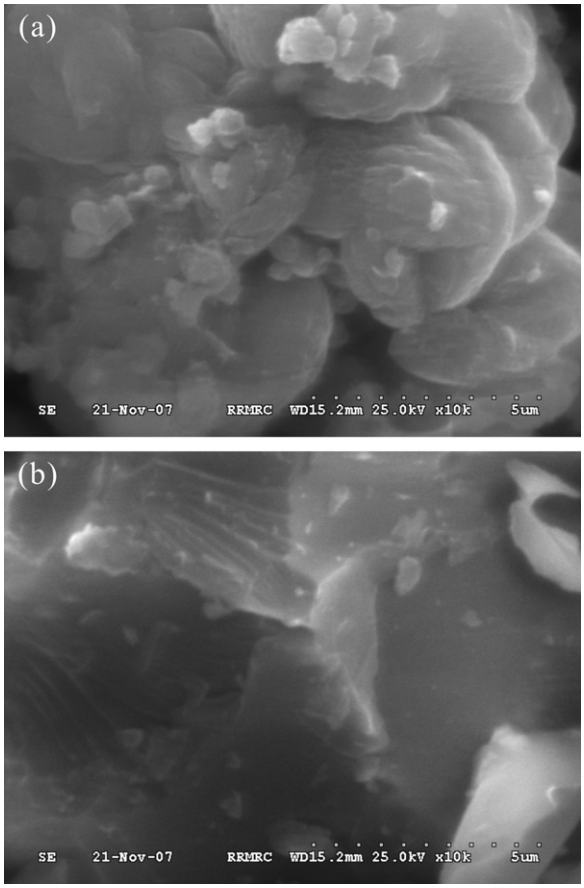

Fig. 7. SEM images of solid specimens: (a) Zn phosphating sludge and (b) slag.

disordered and there were fewer crystals in the glassy matrix. In addition, crystallization is usually regarded as a defect in glass melts [25] and crystals may hinder the material flow in a molten stage and increase the viscosity [26]. The AVF should have an important effect on the viscosity of the melt and may govern the separation of Fe from the glass matrix. However, it needs further investigation to clarify the actual influence of AVF on melt viscosity and iron separation mechanism.

3.5. Leaching and surface characteristics

According to the Identification Standard of Hazardous Materials, the sludge generated from a metal plating process is classified as a hazardous material [27]; therefore, the Zn phosphating sludge is regarded as a hazardous material, regardless of its metal leaching concentration. Nevertheless, TCLP was carried out to evaluate the mobility of hazardous metals in the solid specimens. The TCLP results of the sludge and the slag are listed in Table 5. For the sludge, the Zn leaching concentration was 123 mg/L, but those of other metals were far below the regulated standard. After vitrification, the leached Zn was significantly reduced to non-detectable levels. Overall, no significant difference in metal leaching behavior was observed among slags. Fig. 7 shows the SEM images of the sludge and the slag. The surface morphology of sludge was powdery and spherical. Vitrification transformed such surface structure into an amorphous, bulk, and sharp-edged one, which is preferable for the encapsulation of hazardous metals [28]. The reduction of Zn leaching from the slag can be attributed to the structure transformation and trace amount of Zn due to vaporization.

Table 5
TCLP results (in mg/L) for the sludge and slag.

Element	Sludge	S-1	S-2	S-3	S-4	Regulated limits
Cd	0.053	0.023	0.018	0.040	0.021	1.0
Cr	0.076	N. D.	N. D.	N. D.	N. D.	1.0
Cu	0.026	N. D.	N. D.	N. D.	N. D.	15.0
Mn	0.073	0.197	0.173	0.038	0.245	–
Ni	0.807	0.145	0.219	0.158	0.188	–
Pb	0.115	0.07	0.129	0.054	0.281	5.0
Zn	123	N. D.	N. D.	N. D.	N. D.	–

N.D.: not detectable; –: not available.

4. Conclusion

The Zn phosphating sludge has high level of Fe (81,500 mg/kg) and Zn (73,600 mg/kg). After vitrification, Fe and Zn were predominately separated into the ingot and the particulate phase, respectively. Fe (278,000 mg/kg) existed as Fe_2O_3, Fe_3O_4, and FeP, which can be used as raw materials for iron making. Zn in the coarse (136,000 mg/kg) and the fine (544,000 mg/kg) particulate-phases both existed as ZnO form. For the coarse particulate-phase material, Zn can be reconcentrated by recycling it back into the vitrification furnace. For fine particulate-phase material, the content of ZnO (67.7%) was high enough so that it could be directly sold to metal recovery factories for further refinement. For the slag, the TCLP of metal concentration was far below the regulated standard. Therefore, the recycling of the slag can be taken into consideration. Overall, the result shows that vitrification successfully transformed Zn phosphating sludge into stable slag and separate useful metals as recoverable forms.

Acknowledgement

We acknowledge the financial support by the National Science Council of Taiwan under grant NSC 97-2221-E-273-004-MY3.

References

[1] S. Ilaiyavel, A. Venkatesan, Study on phosphate conversion coating on wear resistance application, J. Eng. Res. Stud. I (2010) 1–4.
[2] T.S.N.S. Narayanan, Surface pretreatment by phosphate conversion coating: a review, Rev. Adv. Mater. Sci. 9 (2005) 130–177.
[3] J.S. Lian, G.Y. Li, L.Y. Niu, C.D. Gu, Z.H. Jiang, Q. Jiang, Electroless Ni–P deposition plus zinc phosphate coating on AZ91D magnesium alloy, Surf. Coat. Technol. 200 (2006) 5956–5962.
[4] J. Donofrio, Zinc phosphating, Met. Finishing 98 (2000) 57–73.
[5] T.J. Weber, Wastewater treatment, Met. Finishing 105 (2007) 699–714.
[6] A.S.M. Ribeiro, R.C.C. Monteiro, E.J.R. Davim, M.H.V. Fernandes, Ash from a pulp mill boiler—characterisation and vitrification, J. Hazard. Mater. 179 (2010) 303–308.
[7] K. Uruga, K. Sawada, Y. Enokida, I. Yamamoto, Vitrification of high-level radioactive waste considering the behavior of platinum group metals, Prog. Nucl. Energy 50 (2008) 514–517.
[8] Y.M. Kuo, J.E. Chang, C.H. Jin, J.Y. Lin, G.P. Chang-Chien, Vitrification for reclaiming spent alkaline batteries, Waste Manag. 29 (2009) 2132–2139.
[9] Y.L. Wei, Y.Y. Lin, J.Q. Yang, H.P. Wang, T.L. Hsiung, Effect of plasma treatment on Ni molecular environment in a spent catalyst and a plating sludge, J. Electron. Spectrosc. Relat. Phenom. 156–158 (2007) 232–235.
[10] H. Ecke, H. Sakanakura, T. Matsuto, N. Tanaka, A. Lagerkvist, Effect of electric arc vitrification of bottom ash on the mobility and fate on metals, Environ. Sci. Technol. 35 (2001) 1531–1536.
[11] Y. Xiao, M. Oorsprong, Y. Yang, J.H.L. Voncken, Vitrification of bottom ash from a municipal solid waste incinerator, Waste Manag. 28 (2008) 1020–1026.
[12] Y.M. Kuo, T.C. Lin, P.J. Tsai, W.J. Lee, H.Y. Lin, Fate of polycyclic aromatic hydrocarbons during vitrification of incinerator ash in a coke bed furnace, Chemosphere 51 (2003) 313–319.
[13] L.L. Oden, W.K. Connor, ASME/US vitrification of residue (ash) from municipal waste combustion systems, Bureau of Mines Investigation Program Report on 1994, 24, ASME Research Committee on Industrial and Municipal Wastes Subcommittee on Ash Vitrification, 1994, p. 49.
[14] C.T. Li, W.J. Lee, K.L. Huang, S.F. Fu, Y.C. Lai, Vitrification of chromium electroplating sludge, Environ. Sci. Technol. 41 (2007) 2950–2956.
[15] National Institute of Environmental Analysis (NIEA), NIEA A302.72C, Standard Method of Detection of Heavy Metals in Outlet Line, Institute of Environmental Analysis (NIEA), Taiwan, 2006, http://www.niea.gov.tw/niea/AIR/A30273C.htm.
[16] U.S. Environmental Protection Agency Method Study 37-SW-846 Method 3050, Acid Digestion of Sediments, Sludges, and Soils, USEPA Contract No. 68-03-3254, 1988.
[17] U.S. Environmental Protection Agency Method 1311, Test Methods for Evaluating Solid Waste Physical/Chemical Methods, SW-846, third ed., Washington, DC, USEPA, 1992.
[18] B.D. Cullity, S.R. Stock, Elements of X-Ray Diffraction, third ed., Prentice Hall, Upper Saddle River, New Jersey, 2001.
[19] C.Y. Chen, G.S. Lan, W.H. Tuan, Preparation of mullite by the reaction sintering of kaolinite and alumina, J. Eur. Ceram. Soc. 20 (2000) 2519–2525.
[20] M. Yellishetty, P.G. Ranjith, A. Tharumarajah, Iron ore and steel production trends and material flows in the world: is this really sustainable, Resour. Conserv. Recycl. 54 (2010) 1084–1094.
[21] G.G. Graf, Primary metals, secondary metals, light metals, in: F. Habashi (Ed.), Handbook of Extractive Metallurgy, VCH Verlagsgesellschaft mbH—A Wiley Company, D-69451 Weinbeim, Federal Republic of Germany, 1997, pp. 641–681.
[22] Y.M. Kuo, T.C. Lin, P.J. Tsai, Metal behavior during vitrification of incinerator ash in a coke bed furnace, J. Hazard. Mater. B109 (2004) 79–84.
[23] S. Jegannathan, T.K. Arumugam, T.S.N.S. Narayanan, K. Ravichandran, Formation and characteristics of zinc phosphate coatings obtained by electrochemical treatment: cathodic vs. anodic, Prog. Org. Coat. 65 (2009) 229–236.
[24] M. Kobya, E. Demirbas, A. Dedeli, M.T. Sensoy, Treatment of rinse water from zinc phosphate coating by batch and continuous electrocoagulation processes, J. Hazard. Mater. 173 (2010) 326–334.
[25] T. Minami, S. Maeda, M.K. Higasa, K. Kashima, In-situ observation of bubble formation at silicon melt–silica glass interface, J. Cryst. Growth 318 (2011) 196–199.
[26] W.D. Kingery, H.K. Bowen, D.R. Uhlmann, Introduction to Ceramics, second ed., John Wiley & Son, Inc., New York, 1976.
[27] Waste Disposal Act: The Standard of Hazardous industrial wastes Identification; EPA://07–0020; Waste/Waste Disposal: 0950098457, Environmental Protection Administration of the Executive Yuan, Taiwan, Republic of China, 2009 (http://law.epa.gov.tw/en/laws/865316921.html).
[28] K. Park, J. Hyun, S. Maken, S. Jang, J.W. Park, Vitrification of municipal solid waste incinerator fly ash using Brown's gas, Energy Fuels 19 (2005) 258–262.